Journal of New Materials for Electrochemical Systems 18, 103-109 (2015)

Electrochemical Performance of $FeF_3 \cdot 0.33H_2O$/MWCNTs Composite Cathode Synthesized by Solvothermal Process

Yanli Zhang[1,2], Li Wang[1,3,†], Jianjun Li[1], Xiangming He[1,*], Lei Wen[4], Jian Gao[1], Hengwei Liu[1], Yufeng Zhang[1] and Peng Zhao[1]

[1]Institute of Nuclear and New Energy Technology, Tsinghua University, Beijing 100084
[2]Shenyang University of Chemical Technology, Shenyang 110142
[3]State Key Laboratory of Automotive Safety and Energy, Tsinghua University, Beijing 100084
[4]Shenyang National Laboratory for Materials Science, Institute of Metal Research, Chinese Academy of Science, Shenyang 110016

Received: November 26, 2014, Accepted: May 04, 2014, Available online: June 30, 2015

Abstract: *This paper reports a $FeF_3 \cdot 0.33H_2O$/multi-walled carbon nanotubes (MWCNTs) composite for energy storage applications. The composite material is prepared by solvothermal reaction with $FeF_3 \cdot 3H_2O$ and MWCNTs as precursors, and $FeF_3 \cdot 3H_2O$ was removed of crystalliferous water and converted to $FeF_3 \cdot 0.33H_2O$ during solvothermal treatment. Structural characterizations show that $FeF_3 \cdot 0.33H_2O$ that crystalline with a diameter of about 30 nm were distributed in the network of MWCNTs. As a cathode material for lithium ion batteries, $FeF_3 \cdot 0.33H_2O$/MWCNTs was superior to pure $FeF_3 \cdot 0.33H_2O$ in terms of high capacity (an initial capacity of 181 mAh g^{-1} in 2.0-4.3 V at 20 mA g^{-1}), good cycleability (50% capacity retension at 50th cycle) and good rate capability (116 mAh g^{-1} at 100 mA g^{-1}). The enhanced performances were attributed to the conductive MWCNT network which improved the electron transport ability and buffered volume change of the cathode.*

Keywords: lithium ion batteries, $FeF_3 \cdot 0.33H_2O$, MWCNTs, composite, electrochemical.

1. INTRODUCTION

There is an increasing demand for lithium ion batteries (LIBs) with higher energy density for electric vehicles and renewable source storage fields [1-3]. The energy density of LIBs is mainly determined by cathode materials. Metal fluorides can store more than one lithium per molecular through both conversion or/and intercalation reactions [4], so their capacities are much larger than commercial $LiCoO_2$ and $LiFePO_4$ materials. In addition, metal fluorides have a high potential brought by the high ionicity of the metal-fluorine bond. Among the different metal fluorides, iron fluoride has a relatively high energy density. Moreover, iron fluoride is abundant and inexpensive and shows good thermal stability at elevated temperatures [5-7]. Iron fluoride is hygroscopic, so hydrates are usually obtained in synthesis [8-10]. A novel ferric fluoride containing a low amount of hydration water ($FeF_3 \cdot 0.33H_2O$) is firstly reported by Li [11], and shows even better electrochemical performance than anhydrous FeF_3.

Unfortunately, iron fluoride is insulating and shows sluggish kinetics during charge/discharge process, which hinders its practical application as cathode in LIBs. Researchers tried a lot to improve iron fluoride's electrochemical performance. As for $FeF_3 \cdot 0.33H_2O$, nanostructuring and controlling of pore structures [11-14] are reported. Graphene oxide [15], CMK-3 [16], acetylene black [9,10,17] and single-walled carbon nanotubes (SWCNTs) [18] also provide a facile electron pathway. Carbon nanotubes, owing to its unique thermal conductivity and mechanical and electrical properties, find wide applications in LIBs. Chilin Li reported a SWCNTs wiring of $FeF_3 \cdot 0.33H_2O$ electrode for LIBs [18]. MWCNTs are another type of carbon nanotubes typically consisting of several tens of coaxial shells [19]. MWCNTs, unlike SWCNTs which would be either metallic or semiconducting depending on their helicities, are always metallic[20-22]. In addition, compared with SWCNTs, MWCNTs can usually be syn-

To whom correspondence should be addressed:
Email: *hexm@tsinghua.edu.cn, †wang-l@tsinghua.edu.cn
Phone: 86 10 62794226; Fax: +86 10 89796031

thesized on a larger scale and at lower cost [23, 24]. The composite of $FeF_3 \cdot 0.33H_2O$ hybridizing with MWCNTs is never reported.

In the literature, $FeF_3 \cdot 0.33H_2O$ is synthesized by two types of methods. One is one-pot synthesis route in which $FeF_3 \cdot 0.33H_2O$ can be generated in one step [10-13, 15-18]. The other route is first synthesis of $FeF_3 \cdot 3H_2O$ and then converting it to $FeF_3 \cdot 0.33H_2O$ by postreatment. The usual postreatment is heat treatment in inert atomosphere at certain temperatures [9, 14, 25]. Here we report converting $FeF_3 \cdot 3H_2O$ to $FeF_3 \cdot 0.33H_2O$ by solvethermal treatment. Solvothermal technique is an effective chemical method to synthesize nanoparticles and nanocomposites with controllable morphology and particle size [26, 27]. This method features for its simple setup and facile operations. Besides, it has been previously reported [28] that solvothermal reaction in ethanol can lead to in situ crystallization and release of bound H_2O from titania sol to generate nanocrystilline TiO_2. In this work, solvothermal process was tried to remove crystalliferous water in $FeF_3 \cdot 3H_2O$. Results showed that most of the crystalliferous water was removed and $FeF_3 \cdot 0.33H_2O$ was generated. Furthermore, MWCNTs were introduced into the solvothermal process and a novel $FeF_3 \cdot 0.33H_2O$/MWCNTs composite was synthesized. The microstructures are characterized by SEM, TEM and Thermogravimetry (TGA). The electrochemical properties of $FeF_3 \cdot 0.33H_2O$/MWCNTs composite are compared with pure $FeF_3 \cdot 0.33H_2O$.

2. EXPERIMENTAL

2.1. Synthesis of $FeF_3 \cdot 3H_2O$

$FeF_3 \cdot 3H_2O$ particles were synthesized by a simple liquid-phase method, modified from a previously reported procedure [29]. 25 mL of NH_4HF_2 aqueous solution (1.5 M) was introduced to 100 mL of $Fe(NO_3)_3 \cdot 9H_2O$ ethanol solution (0.25 M) dropwise, followed by vigorous stirring for 2h to complete the reaction. The product ($FeF_3 \cdot 3H_2O$) was washed and harvested with ethanol by centrifugation. $FeF_3 \cdot 3H_2O$ particles were used as one of precursors for synthesis of $FeF_3 \cdot 0.33H_2O$/MWCNTs in the following solvothemal process.

2.2. Synthesis of $FeF_3 \cdot 0.33H_2O$/MWCNTs

MWCNTs were provided by Wei (China) and produced by a chemical vapor deposition (CVD) technique using iron as the catalyst [22]. As-received MWCNTs were refluxed in a mixed acid solution (HNO_3 and H_2SO_4 in a volume ratio of 3:1) at 120 °C for 3h for purification and for its easy dissolution into ethanol [30, 31]. 1.44 g $FeF_3 \cdot 3H_2O$ and 0.18 g treated MWCNTs were added to 45 mL ethanol in a glass beaker. The dispersion was tip-sonicated for 30 min. Then the suspension was transferred into a 50 mL telfon-lined stainless-steel autoclave and sealed. The autoclave was put into an electric oven and kept at 120 °C for 10h. After the solvothermal treatment, the produced sample was collected by filtration and washed thoroughly with ethanol. The $FeF_3 \cdot 0.33H_2O$/MWCNTs sample was finally dried at 80 °C for 10h for further characterization. For comparative purposes, pure $FeF_3 \cdot 0.33H_2O$ was prepared by the same procedure as described above except for the addition of MWCNTs.

2.3. Morphology and structure characterization

The phase of the sample was characterized by X-ray diffraction (XRD) using D8 ADVANCE (3 KW) with Cu-K radiation. The morphology was investigated by a scanning electron microscope (SEM, Sirion 200) instrument. The microstructure of the sample was characterized by a transmission electron microscopy (TEM, JEOL JEM-2010). TGA was carried out with a NETZSCH STA 409PC in air from 30 °C to 1150 °C at a heating rate of 10 °C min^{-1} to investigate the content of MWCNTs in the $FeF_3 \cdot 0.33H_2O$/MWCNTs composite.

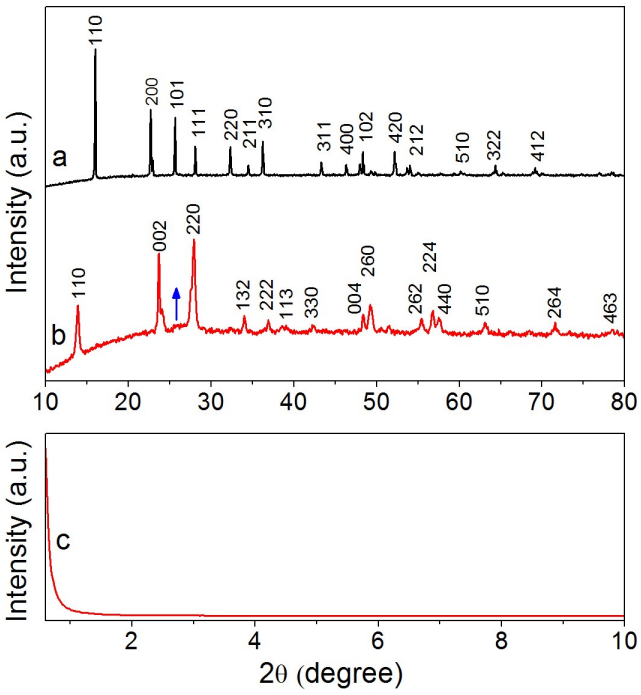

Figure 1. XRD patterns of $FeF_3 \cdot 3H_2O$ (a) and the $FeF_3 \cdot 0.33H_2O$/MWCNTs composite (b), the shoulder peak marked by the blue arrow originates from MWCNTs. Low angle XRD pattern of the the $FeF_3 \cdot 0.33H_2O$/MWCNTs composite (c).

2.4. Electrochemical measurements

Two-electrode coin-type cells were utilized to evaluate the electrochemical performances of the cathode composite. The cells were assembled in an Ar-filled glove box with a working electrode, a lithium foil counter electrode and a porous separator (Celgard 2500). The working electrode was prepared by mixing active material, acetylene black and Poly (tetrafluoroethene) (PTFE) at a weight ratio of 80:10:10, which were then suppressed and punched into a small disk followed by drying in vacuum at 120 °C for 24 h. The electrolyte involves 1 M $LiPF_6$ in a non-aqueous electrolyte of ethylene carbonate (EC), dimethyl carbonate (DMC) and metal ethyl carbonate (EMC) with a volume ratio of 1:1:1. The cells were galvanostatically charged and discharged using a battery test system (LAND CT2001A model, Wuhan Jinnuo Electronics Co. Ltd.) at different current rates between 2.0 and 4.3 V versus Li/Li^+. The electrochemical impedance spectroscopy (EIS) of the cells was performed over the frequency range between 1 MHz and 100 mHz with the amplitude of an AC signal of 5 mV on an IM6 ex electrochemical workstation.

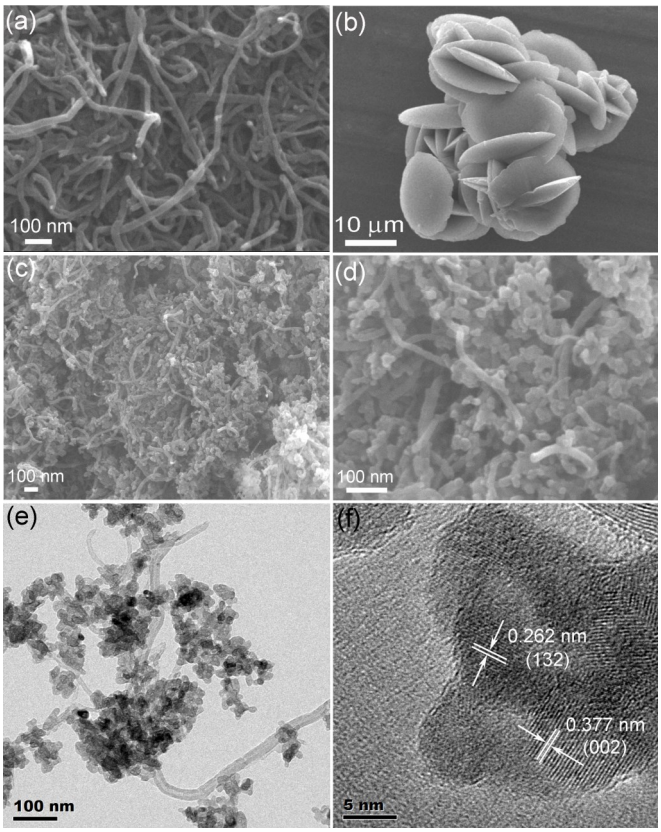

Figure 2. SEM images of MWCNTs (a) and $FeF_3 \cdot 3H_2O$ (b) and $FeF_3 \cdot 0.33H_2O$/MWCNTs composite (c, d). TEM image of $FeF_3 \cdot 0.33H_2O$/MWCNTs composite (e). HRTEM imageof $FeF_3 \cdot 0.33H_2O$ nanocrystalline in the composite (f).

3. RESULTS AND DISCUSSION

Fig. 1 shows the XRD patterns of $FeF_3 \cdot 3H_2O$ (a) and the $FeF_3 \cdot 0.33H_2O$/MWCNTs composite (b). All peaks in Fig. 1a can be assgined to a pure tetragonal $FeF_3 \cdot 3H_2O$ (JCPDS: 32-0464). The diffraction peaks in Fig. 1b can be indexed to a well-crystallined base-centered $FeF_3 \cdot 0.33H_2O$ (JCPDS: 76-1262) and a very small intensity reflection around 26 θ degree due to the presence of MWCNTs can be observed. No diffraction peaks corresponding to the precursor phase $FeF_3 \cdot 3H_2O$ can be observed. We have also measured the low angle XRD pattern of the $FeF_3 \cdot 0.33H_2O$/MWCNTs composite to see if there is FeF_2 formation or not. As shown in Fig. 1 (c), there is not any peaks in the pattern. So there is no FeF_2 formation during the solvothermal process and FeF_2 doesn't exist in the $FeF_3 \cdot 0.33H_2O$/MWCNTs composite. The XRD results indicate that the $FeF_3 \cdot 3H_2O$ precursor lost most of the crystalliferous water during solvothermal process and re-crystallized and converted into $FeF_3 \cdot 0.33H_2O$ thoroughly.

The particle size and morphology of the $FeF_3 \cdot 0.33H_2O$/MWCNTs composite are characterized by SEM. The SEM image in Fig. 2a shows that the MWCNTs is pure and the diameter is in the range of 20-30 nm. Fig. 2b shows that $FeF_3 \cdot 3H_2O$ has a morphology of disk-like shapes with diameters of about 10 μm and thickness of several hundreds of nanometers, and most of disk-like particles interweave like a propeller tip. On the other hand, SEM images (Fig. 2c and d) of the $FeF_3 \cdot 0.33H_2O$/MWCNTs composite reveal that $FeF_3 \cdot 0.33H_2O$ are nanocrystallines with a particle size of about 30 nm, and MWCNTs are uniformly distributing in the composite. TEM observation (Fig. 2e) further verify that the nanocrystallines are well mixed with MWCNTs and $FeF_3 \cdot 0.33H_2O$ nanocrystallines adhere on every MWCNT. A high resolution TEM image of a $FeF_3 \cdot 0.33H_2O$ nanocrystalline is shown in Fig. 2f. Two sets of lattice fringes around the particle boundary can be seen, indicating that the $FeF_3 \cdot 0.33H_2O$ nanocrystalline is polycrystalline. The two inter-planar (*d*) spacings are 0.262 nm and 0.377 nm, corresponding to the (132) and (002) lattice plane of $FeF_3 \cdot 0.33H_2O$, respectively. Fig. 2f also shows that there are pores inside the $FeF_3 \cdot 0.33H_2O$ nanocrystalline, which may be derived from losing of crystalliferous water and re-crystallization from $FeF_3 \cdot 3H_2O$ particles.

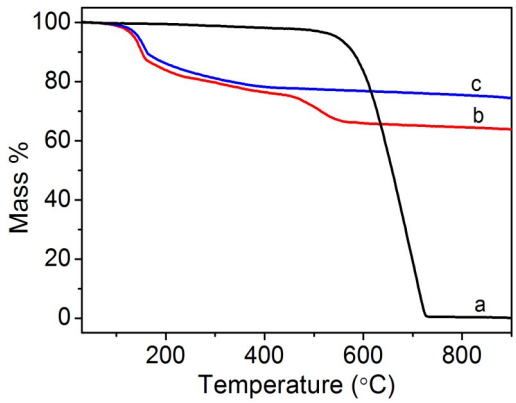

Figure 3. TGA curves of the MWCNTs (a), the $FeF_3 \cdot 0.33H_2O$/MWCNTs (b), and pure $FeF_3 \cdot 0.33H_2O$ (c) at 10 °C/min in air.

The amount of $FeF_3 \cdot 0.33H_2O$ in the $FeF_3 \cdot 0.33H_2O$/MWCNTs composite was quantitatively analyzed by TGA curves as shown in Fig.3. The oxidation of MWCNTs took place between 450 and 710 °C and the residual weight is 0 wt.%. The weight loss of pure $FeF_3 \cdot 0.33H_2O$ happened in three steps. The weight loss (~11 wt.%) in the range of 115-163 °C can be ascribed to the self oxidation of $FeF_3 \cdot 0.33H_2O$ by the crystalliferous water. A weigh loss (12 wt.%) in 163-420 °C was attributed to the partial oxidation of FeF_3 into Fe_2O_3 by oxygen. The slight weigh loss (3wt.%) in 420-963 °C is due to the further oxidation of FeF_3, and the slow oxidation rate results from the Fe_2O_3 limiting oxygen penetration and reaction with the residual FeF_3. The residual weight was 74.5 wt.% by 900 °C. By comparing the TG curve of the $FeF_3 \cdot 0.33H_2O$/MWCNTs composite with that of pure $FeF_3 \cdot 0.33H_2O$, it is found that the weight loss in the ranges of 115-163, 163-420, and 558-900 °C are similar between the two samples, so we owe the weight loss of the $FeF_3 \cdot 0.33H_2O$/MWCNTs composite in the above three ranges to the oxidation of $FeF_3 \cdot 0.33H_2O$ in the composite. Besides, the TG curve of the composite contains a weight loss in 450-558 °C, which was mainly attributed to the oxidation of MWCNTs. The residual weight of the $FeF_3 \cdot 0.33H_2O$/MWCNTs composite is 63.4 wt.%,

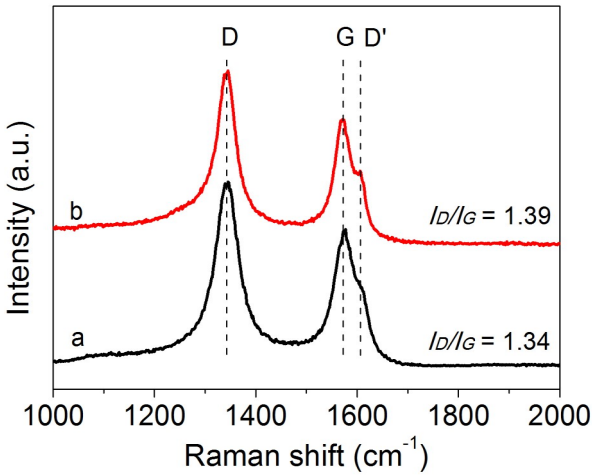

Figure 4. Raman spectra of the MWCNTs (a) and the $FeF_3 \cdot 0.33H_2O$/MWCNTs (b)

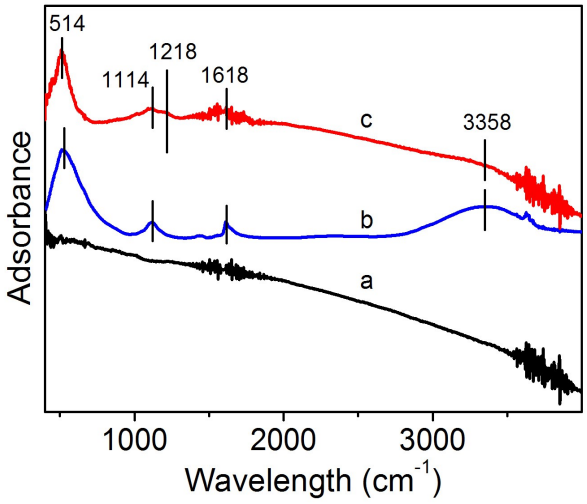

Figure 5. FTIR spectra of MWCNTs (a), pure $FeF_3 \cdot 0.33H_2O$ (b) and the $FeF_3 \cdot 0.33H_2O$/MWCNTs ©

and the final residues have the same composition with the pure $FeF_3 \cdot 0.33H_2O$. So the weight content of $FeF_3 \cdot 0.33H_2O$ in the $FeF_3 \cdot 0.33H_2O$/MWCNTs composite = 63.4 wt.% / 74.5 wt.% = 85.2 wt.%. The weight content of MWCNTs is 14.8 wt.%, which was roughly in agreement with the original feed ratio before the solvothermal process.

Fig.4 shows raman spectra of MWCNTs and the $FeF_3 \cdot 0.33H_2O$/MWCNTs composite. Two major bands locating at 1347 and 1576 cm^{-1} and a shoulder band locating at 1606 cm^{-1} are observed, which can be assigned to a disorder-induced phonon mode (D band), the in-plane sp^2 vibration (G band) and D' band [32], respectively. The relative intensity (I_D/I_G) of the D band and the G band of the two samples are compared. The I_D/I_G of the MWCNTs is 1.34, and the changes are not distinct after forming composites. The slight increase of the D/G ratio in the $FeF_3 \cdot 0.33H_2O$/MWCNTs composite is spectulated to derive from the following two reseaons: defects may formed on walls of MWCNTs during the solvothermal process; the surfaces of the MWCNTs may be bonded with the $FeF_3 \cdot 0.33H_2O$ nanoparticles' surfaces.

Fig.5 shows the FTIR spectra of the MWCNTs, pure $FeF_3 \cdot 0.33H_2O$ and the $FeF_3 \cdot 0.33H_2O$/MWCNTs. There isn't any obvious IR absorption bands for the MWCNTs, which was speculated due to the strong adsorption of MWCNTs itself. The easy dissolution of the MWCNTs into ethanol before solvothermal process proves the existance of some functional group on CNTs' surface. By comparing the spectra of $FeF_3 \cdot 0.33H_2O$/MWCNTs with that of pure $FeF_3 \cdot 0.33H_2O$, it was found that both spectra contain absorption peaks at 514, 1114, 1618 and 3358 cm^{-1}. The signal at 514 cm^{-1} can be attributed to the bending vibration of the Fe-F bond in $FeF_3 \cdot 0.33H_2O$[33, 34], and the signal at 1618 and 3358 cm^{-1} can be attributed to the vibration of H-O-H and –OH in the crystallious water of $FeF_3 \cdot 0.33H_2O$ [35, 36]. Apart from the above peaks, there is a signal at 1218 cm^{-1} in the spectrum of $FeF_3 \cdot 0.33H_2O$/MWCNTs only, and the signal was assigned to the vibration of the C-F bond [37, 38]. This result indicates that the $FeF_3 \cdot 0.33H_2O$ particles are covalently attached to MWCNTs in the composite.

Electrochemical performance of the $FeF_3 \cdot 0.33H_2O$/MWCNTs composite was evaluated using half cell. For comparison, pure $FeF_3 \cdot 0.33H_2O$ was also tested. Fig. 6a shows the initial discharge and charge profiles of $FeF_3 \cdot 0.33H_2O$/MWCNTs and $FeF_3 \cdot 0.33H_2O$ in the voltage range of 2.0-4.3 V at a current density of 20 mA g^{-1}. Both discharge curves of the two samples show sloped reaction around 3.0 V, which mainly stem from Li^+ insertion into the $FeF_3 \cdot 0.33H_2O$ nanocrystalline forming $LiFeF_3.0.33H_2O$ [11]. The initial discharge capacitis of $FeF_3 \cdot 0.33H_2O$/MWCNTs and pure $FeF_3 \cdot 0.33H_2O$ is 180.9 mAh g^{-1} and 119.9 mAh g^{-1}, respectively. The initial discharge capacity of $FeF_3 \cdot 0.33H_2O$/MWCNTs is higher than the full theoretical capacity of $FeF_3 \cdot 0.33H_2O$, and it is spectulated that a conversion reaction occurs in the first discharge process [39, 40] and contributes to the extra capacity.

Fig. 6b shows the cyclic performances of $FeF_3 \cdot 0.33H_2O$ /MWCNTs and pure $FeF_3 \cdot 0.33H_2O$. $FeF_3 \cdot 0.33H_2O$/MWCNTs reaches stabilization after about 10 cycles and remains capable of delivering 90.5 mAh g^{-1} at the 50th cycle, while the $FeF_3 \cdot 0.33H_2O$ electrode is roughly stabilized after about 20 cycles and only 29.4 mAh g^{-1} is delivered after 50 cycles. The capacity of $FeF_3 \cdot 0.33H_2O$/MWCNTs after stabilization is lower than the theoretical capacity of $FeF_3 \cdot 0.33H_2O$. The reason lies that although most $FeF_3 \cdot 0.33H_2O$ nanoparticles adhere on the walls of MWCNTs, there are still a few nanoparticles aggregate together and aren't in good electrical contact with the conductive MWCNTs. In this sense, further increasing the dispersion of $FeF_3 \cdot 0.33H_2O$ nanoparticles and making them evenly attach to the MWCNTs' walls will be beneficial and will be explored in future.

Furthermore, as shown in Fig. 6c, $FeF_3 \cdot 0.33H_2O$/MWCNTs exhibits better rate capability with discharge capacities of 138 mAh g^{-1} at 50 mA g^{-1}, 116 mAh g^{-1} at 100 mA g^{-1}, and 86 mAh g^{-1} at 250 mA g^{-1}; $FeF_3 \cdot 0.33H_2O$ can only maintain discharge capacities of 74 mAh g^{-1} at 50 mA g^{-1}, 59 mAh g^{-1} at 100 mA g^{-1}, and 29 mAh g^{-1} at 250 mA g^{-1}.

From the above electrochemical results, it can be seen that

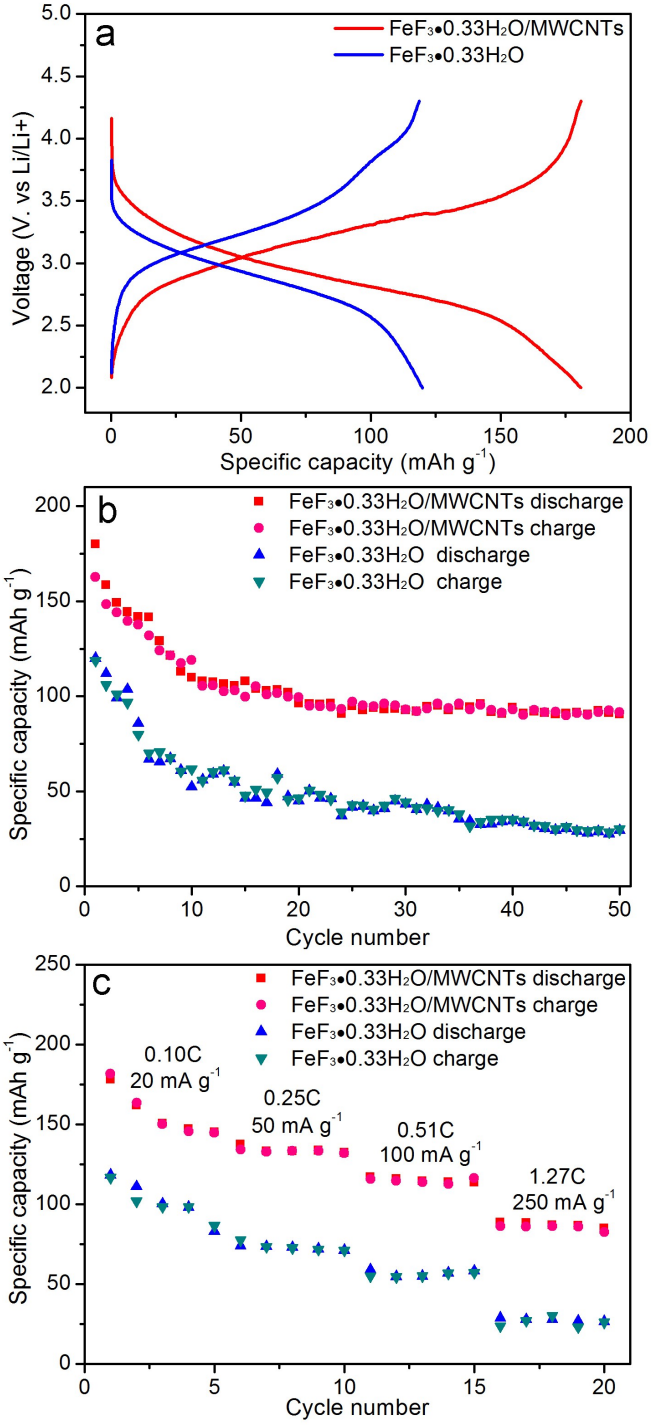

Figure 6. Initial galvanostatic discharge-charge voltage profiles (a), cycling performance (b) (vs. Li^+/Li) at a current of 20 mA $g^{-1}$and rate performance (c) of the $FeF_3 \cdot 0.33H_2O$/MWCNTs composite and pure $FeF_3 \cdot 0.33H_2O$ in the voltage of 2.0-4.3 V.

$FeF_3 \cdot 0.33H_2O$/MWCNTs displays great improvement on specific capacities, cyclic and rate capability in comparison to pure $FeF_3 \cdot 0.33H_2O$, which verified the effectiveness of MWCNTs modification on improving the electrochemical performance of the material. To understand the reasons for the improved performance of $FeF_3 \cdot 0.33H_2O$/MWCNTs, electrochemical impedance spectra (EIS) measurements were carried out (Fig. 7). The moderate-high frequency semicircle is related to the charge transfer resistance (R_{ct}); the inclined linear part at low frequencies represents the Warburg impedance (W_z) that is related to lithium ion diffusion in electrode materials. The intercept at the Z' real axis at high frequency corresponds to the ohmic resistance (R_s). The simplified equivalent circuit mode[17, 25, 41] of the Nyquist plots was shown in the inset of Fig. 5. The capacitance (C) in the mode is related to the interfacial resistance. The R_s = 9.812 Ω of the $FeF_3 \cdot 0.33H_2O$/MWCNTs is smaller than R_s = 34.797 Ω of the pure $FeF_3 \cdot 0.33H_2O$. Moreover, $FeF_3 \cdot 0.33H_2O$/MWCNTs has lower charge transfer resistance (R_{ct} = 632 Ω) than that of $FeF_3 \cdot 0.33H_2O$ (R_{ct} = 1175 Ω). The EIS results imply that $FeF_3 \cdot 0.33H_2O$/MWCNTs possess higher conductivity and faster charge transfer during electrochemial process.

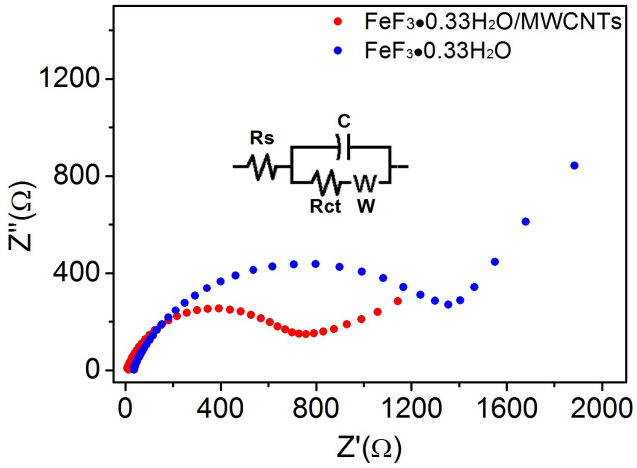

Figure 7. EIS spectra of the $FeF_3 \cdot 0.33H_2O$/MWCNTs composite and pure $FeF_3 \cdot 0.33H_2O$ after assembly and a 36 h rest. (inset: the simplified equivalent circuit mode).

The improved electrochemical performance of $FeF_3 \cdot 0.33H_2O$/MWCNTs are considered to originated from the following three factors. First, most of the $FeF_3 \cdot 0.33H_2O$ nanoparticles have good electrical contact with MWCNTs, and the cross-linked MWCNTs form an electrical conductive network, so the overall electrical conductivity of the electrode is improved. Second, the MWCNTs also produce much easier charge transfer at the electrode-electrolyte interface and further decrease the overall internal resistance. Third, the volume expansion/contraction of $FeF_3 \cdot 0.33H_2O$ nanoparticles during electrochemical process can be buffered by the flexible MWCNTs to some extent.

The influence of MWCNT content on the electrochemical performance of the composite is investigated. Fig. 8 depicts the initial charge/discharge curves for the composite with various MWCNT contents. All the samples exhibited similar voltage plateaus, but their initial capacities are different. With an increase in the MWCNT content from 5 to 15 wt.%, the discharge capacity of the composite was improved from 162 to 181 mAh g^{-1}, which can be ascribed that higher MWCNT content bring better electronic con-

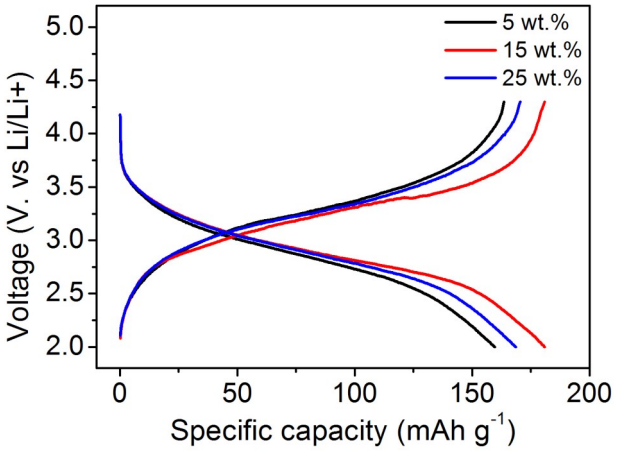

Figure 8. Charge and discharge profiles for the $FeF_3 \cdot 0.33H_2O$/MWCNTs composite with various MWCNTs contents.

ductivity, and further higher capacity. When MWCNT content increased to 25 wt.%, the discharge capacity dropped to 170 mAh g^{-1}, which could be attributed to the fact that too much $FeF_3 \cdot 0.33H_2O$ was subsituted by excessive MWCNTs and resulted of the decrease of theoretic capacity. Thus, the composite with ~15 wt.% of MWCNT content was optimum and shows well discharge capacity.

4. CONCLUSION

The $FeF_3 \cdot 0.33H_2O$/MWCNTs composite was successfully synthesized through a solvothermal process with $FeF_3 \cdot 3H_2O$ and MWCNTs as precursors. $FeF_3 \cdot 3H_2O$ lost most of its crystalliferous water and recrystallized and converted to $FeF_3 \cdot 0.33H_2O$ during solvothermal treatment. In the composite, the $FeF_3 \cdot 0.33H_2O$ nanocrystallines have a particle size of about 30 nm, and most of them adhere on the MWCNTs walls. The content of MWCNTs in the composite is about 15 wt.%, and MWCNTs retained most of its structural integrity during solvothermal treatment. There is weak bond between $FeF_3 \cdot 0.33H_2O$ and MWCNTs. The composite exhibited an initial capacity of 181 mAh g^{-1} and delivered 90.5 mAh g^{-1} at 50th cycle at 20 mA g^{-1} in 2.0-4.3 V, which is much better than pure $FeF_3 \cdot 0.33H_2O$. The solvothermal route provides a new way for post treatment of substances with crystalliferous water.

5. ACKNOWLEDGEMENT

This work is supported by the MOST (Grant No. 2011CB935902, No. 2013CB934000, No. 2013AA050903 and No. 2010DFA72760) and the Tsinghua University Initiative Scientific Research Program (Grant No. 2010THZ08116, No. 2011THZ08139, No. 2011THZ01004 and No. 2012THZ08129) and State Key Laboratory of Automotive Safety and Energy (Grant No. ZZ2012-011).

REFERENCES

[1] J. M. Tarascon, Philos T R Soc A, 368, 3227 (2010).
[2] M. M. Thackeray, C. Wolverton and E. D. Isaacs, Energ Environ Sci, 5, 7854 (2012).
[3] B. Dunn, H. Kamath and J. M. Tarascon, Science, 334, 928 (2011).
[4] G. G. Amatucci and N. Pereira, J Fluorine Chem, 128, 243 (2007).
[5] M. J. Zhou, L. W. Zhao, A. Kitajou, S. Okada and J. Yamaki, J Power Sources, 203, 103 (2012).
[6] M. J. Zhou, L. W. Zhao, S. Okada and J. Yamaki, J Power Sources, 196, 8110 (2011).
[7] M. J. Zhou, L. W. Zhao, T. Doi, S. Okada and J. Yamaki, J Power Sources, 195, 4952 (2010).
[8] C. L. Li, C. L. Yin, L. Gu, R. E. Dinnebier, X. K. Mu, P. A. van Aken and J. Maier, J Am Chem Soc, 135, 11425 (2013).
[9] L. Liu, H. P. Guo, M. Zhou, Q. L. Wei, Z. H. Yang, H. B. Shu, X. K. Yang, J. L. Tan, Z. C. Yan and X. Y. Wang, J Power Sources, 238, 501 (2013).
[10]X. P. Xu, S. Chen, M. Shui, L. X. Xu, W. D. Zheng, J. Shu, L. L. Cheng, L. Feng and Y. L. Ren, Ceram Int, 40, 3145 (2014).
[11]C. L. Li, L. Gu, S. Tsukimoto, P. A. van Aken and J. Maier, Adv Mater, 22, 3650 (2010).
[12]C. L. Li, L. Gu, J. W. Tong, S. Tsukimoto and J. Maier, Adv Funct Mater, 21, 1391 (2011).
[13]B. J. Li, Z. J. Cheng, N. Q. Zhang and K. N. Sun, Nano Energy, 4, 7 (2014).
[14]J. Liu, W. Liu, S. M. Ji, Y. L. Wan, M. Z. Gu, H. Q. Yin and Y. C. Zhou, Chem-Eur J, 20, 5815 (2014).
[15]L. Di Carlo, D. E. Conte, E. Kemnitz and N. Pinna, Chem Commun, 50, 460 (2014).
[16]B. J. Li, N. Q. Zhang and K. N. Sun, Small, 10, 2039 (2014).
[17]J. L. Tan, L. Liu, H. Hu, Z. H. Yang, H. P. Guo, Q. L. Wei, X. Yi, Z. C. Yan, Q. Zhou, Z. F. Huang, H. B. Shu, X. K. Yang and X. Y. Wang, J Power Sources, 251, 75 (2014).
[18]C. L. Li, L. Gu, J. W. Tong and J. Maier, Acs Nano, 5, 2930 (2011).
[19]T. W. Ebbesen and P. M. Ajayan, Nature, 358, 220 (1992).
[20]R. Martel, T. Schmidt, H. R. Shea, T. HertelandP. Avouris, Appl Phys Lett, 73, 2447 (1998).
[21]T. W. Odom, J. L. Huang, P. Kim and C. M. Lieber, Nature, 391, 62 (1998).
[22]Y. Wang, F. Wei, G. H. Luo, H. Yu and G. S. Gu, Chem Phys Lett, 364, 568 (2002).
[23]M. Kumar and Y. Ando, Chem Phys Lett, 374, 521 (2003).
[24]L. P. Biro, Z. E. Horvath, L. Szalmas, K. Kertesz, F. Weber, G. Juhasz, G. Radnoczi and J. Gyulai, Chem Phys Lett, 372, 399 (2003).
[25]L. Liu, M. Zhou, L. H. Yi, H. P. Guo, J. L. Tan, H. B. Shu, X. K. Yang, Z. H. Yang and X. Y. Wang, J Mater Chem, 22, 17539 (2012).
[26] L. Wang, X. M. He, W. T. Sun, J. L. Wang, Y. D. Li and S. S. Fan, Nano Lett, 12, 5632 (2012).
[27] L. Wang, W. T. Sun, X. Y. Tang, X. K. Huang, X. M. He, J. J. Li, Q. W. Zhang, J. Gao, G. Y. Tian and S. S. Fan, J Power Sources, 244, 94 (2013).

[28] J. Cao, L. Wang, X. M. He, M. Fang, J. Gao, J. J. Li, L. F. Deng, H. Chen, G. Y. Tian, J. L. Wang and S. S. fan, J Mater Chem A, 1, 5955 (2013).
[29] T. Li, L. Li, Y. L. Cao, X. P. Ai and H. X. Yang, J Phys Chem C, 114, 3190 (2010).
[30] A. Pistone, A. Ferlazzo, M. Lanza, C. Milone, D. Lannazzo, A. Piperno, E. Piperopoulous and S. Galvagno, Journal of Nanoscience and Nanotechnology, 12, 5054 (2012).
[31] N. T. Hung, I. V. Anoshkin, A. P. Dementjev, D. V. Katorov and E. G. Rakov, Inorganic Materials, 44, 219 (2008).
[32] A. C. Ferrari and J. Robertson, Phys Rev B, 64, 075414 (2001).
[33] Y. P. Zhao, X. Y. Li, L. Liu and F. H. Chen, Carbohydrate Polymers, 72, 144 (2008).
[34] J. Liang, A. Safriet, S. Briley and M. Roselius, J Fluorine Chem, 79, 53 (1996).
[35] W. Z. Xu, C. T. Johnston, P. Parker and S. F. Agnew, Clays and Clay Minerals, 48, 120 (2000).
[36] B. J. Saikia and G. Parthasarathy, Journal of Modern Physics, 1, 206 (2010).
[37] G. S. Kang, H. J. Ko, C. K. Choi and C. S. Chang, Journal of the Korean Physical Society, 42, 676 (2003).
[38] P. K. Reddy, K. Mukkanti and D. M. Rao, Oriental Journal of Chemistry, 29, 1015 (2013).
[39] Y. Ma and S. H. Garofalini, J Am Chem Soc, 134, 8205 (2012).
[40] F. Wang, R. Robert, N. A. Chernova, N. Pereira, F. Omenya, F. Badway, X. Hua, M. Ruotolo, R. G. Zhang, L. J. Wu, V. Volkov, D. Su, B. Key, M. S. Whittingharn, C. P. Grey, G. G. Amatucci, Y. M. Zhu and J. Graetz, J Am Chem Soc, 133, 18828 (2011).
[41] X. L. Li, F. Y. Kang, X. D. Bai and W. Shen, Electrochem Commun., 9, 663 (2007).